Irregular scattering and quantum transport fluctuations

1992 J. Phys. A: Math. Gen. 25 3239

(http://iopscience.iop.org/0305-4470/25/11/028)

J. Phys. A: Math. Gen. 25 (1992) 3239–3259. Printed in the UK

Irregular scattering and quantum transport fluctuations

Fausto Borgonovi†‡ and Italo Guarneri‡§

† Dipartimento di Fisica Nucleare e Teorica dell'Universita' di Pavia, via Bassi 6, 27100 Pavia, Italy

‡ Istituto Nazionale di Fisica Nucleare, Sezione di Pavia, via Bassi 6, 27100 Pavia, Italy

§ Università di Milano, sede di Como, via Castelnuovo, 22100 Como, Italy

Received

Abstract. We study a one-dimensional abstract model for classical and quantum irregular scattering in which the interacting dynamics is defined by the standard map. This model allows for a direct comparison of classical and quantum transport properties. Whereas the classical model is characterized by chaotic diffusion, in the quantum case the interplay of diffusion and localization determines a transition from a ballistic regime to a localized one, with an intermediate ohmic regime in the crossover region. The scattering matrix is numerically computed by solving a Lippman–Schwinger equation. In the ballistic regime the S-matrix fluctuations are found to share some typical features with the Ericson fluctuations, with correlation lengths close to the classical rates of exponential decay. Qualitative modifications occurring in the diffusive regime, including universal transmission fluctuations, are discussed.

1. Introduction

The foundational relevance of the classical doctrine of chaos is largely due to its provision of sound foundations for non-equilibrium statistical mechanics even for systems with a small number of freedoms. For this reason, the possible persistence of chaotic features in quantum mechanics is an important issue in the study of quantum transport phenomena that involve only a small number of particles.

One such phenomenon is the behaviour of the residual resistance of disordered solids, which is usually investigated in terms of single-particle dynamics in a disordered potential. In Landauer's approach, the conduction of electrons through one- and quasi-one-dimensional disordered solids is pictured as a scattering process (Landauer 1970, Buttiker *et al* 1985, Pichard 1986), so that in this type of problem one has to deal simultaneously with quantum scattering and quantum transport.

The peculiarities of quantum scattering when the dynamics inside the interaction region is classically chaotic are now a subject of widespread interest. After Gutzwiller's (1983) study of scattering on a variety of negative curvature, a number of different model systems have been extensively studied (Gaspard and Rice 1989, Eckardt and Cvitanovic 1989, Blumel and Smilansky 1988). A connection between classical chaotic decay rates and quantum resonance widths has been clearly established (Gaspard and Rice 1989, Eckardt and Cvitanovic 1989); moreover, the important surmise has been formulated that the appearance of cross section fluctuations similar to those that go under Ericson's name in nuclear physics (Brody *et al* 1981) is a generic

0305-4470/92/113239+21$04.50

quantum signature of classical chaos in the regime of strongly overlapping resonances (Smilansky 1990).

All this leads to an interesting question. It is well known that the residual conductance of mesoscopic devices exhibits strong fluctuations in the weakly localized regime (see, for example, Vollhardt (1987)); moreover, the statistical methods from random matrix theory, already used in the analysis of nuclear Ericson fluctuations, have been extended to the description of such 'mesoscopic fluctuations' (Bohigas and Weidenmuller 1988). This makes it all the more natural to inquire whether mesoscopic fluctuations can also be reduced within the framework of chaotic Ericson-like fluctuations (Casati *et al* 1990, Bohigas and Weidenmuller 1988, Smilansky 1990).

In order to address this problem, one needs a quantum model endowed with a well-defined classical limit in which a chaotic diffusive transport takes place according to Ohm's law. The usual models do not satisfy these requirements, either because their classical limits are not well defined (as in tight-binding quantum models) or because these classical limits, though chaotic, are not diffusive. In fact, whereas diffusion would require classical decay times significantly larger than the chaotization time, hitherto investigated models have these two times roughly on the same order.

In order to obtain chaotic diffusion in a model with elastic scattering, two spatial dimensions (at least) and a large number of scatterers are needed, which makes a proper quantum simulation a considerable computational task.

In this paper we present a much simpler model, which in spite of a seemingly unphysical character, conveys some essential features of the problem. This model is once more a variant of the standard map, better known in its quantum version as the kicked rotator (KR). As is well known this model exhibits the two essential properties of classical and quantum transport, i.e. classical chaotic diffusion and quantum localization; indeed, its similarity to one-dimensional models for quantum transport has, up until now, been successfully implemented in order to get an understanding of its dynamical properties (Fishman *et al* 1982, Blumel *et al* 1987)).

We now reverse this approach and use the KR as a model for both one-dimensional transport and chaotic scattering. In our scattering model the interacting dynamics is defined by the standard map, and if the interaction region is sufficiently extended, the chaotic transport across it has a diffusive character. In spite of the complete absence of external random agents, this transport is statistically well described by a Fokker–Planck boundary-value problem that yields an explicit formula for the classical transmission coefficient. This formula is in excellent agreement with the results of numerical simulations and shows that the classical transport has an 'ohmic' character. 'Ohmic' here means that the transmission coefficient is inversely proportional to the length of the sample; a direct definition of conductance for our model will not be attempted here—this may look somewhat artificial in view of the abstract nature of the model itself.

In the quantum model, the transport coefficients are directly and self-consistently defined from the scattering matrix, which can be numerically computed with good accuracy. A direct comparison of classical and quantum transport properties is thus made possible, without recourse to phenomenological assumptions on either side.

A number of interesting questions can be conveniently analysed in this way. Besides providing a new illustration of the well-known localization effect occurring in the quantum standard map, this approach allows the transition to the delocalized 'metallic' regime to be investigated. It turns out that in between the extreme cases represented by the ballistic and localized regimes, room is left for a quantum ohmic regime.

Finally, we report on numerical investigations of the S-matrix fluctuations in the 'metallic' regime of strong delocalization, aimed at investigating whether these fluctuations have an Ericson character, as S-matrix fluctuations have been found to have in other classically chaotic scattering problems. This turned out to be the case in the ballistic regime, where the sample size is comparable with or less than the mean free path; here the observed S-matrix fluctuations are approximately Lorentz-correlated with correlation lengths approximately equal to the classical diffusive decay rates (inverse escape times). Similar indications have already been given by other authors (Jalabert *et al* 1990), who investigated the ballistic regime in a different model for Ericson-like fluctuations in mesoscopic devices.

The metallic *diffusive* regime, where the sample size is significantly larger than the mean free path, was found to be qualitatively different. Here our results indicate that the correlation lengths of S-matrix fluctuations are significantly higher than the classical diffusive decay rates. How does the thickness of fluctuations depend on the relevant parameters in this regime is an open theoretical question. Nevertheless, the size of the fluctuations of the transmission coefficient that are observed upon changing various parameters is practically scale-independent in the ohmic regime, in close parallel with the universal conductance fluctuations of solid state physics.

Other important issues such as the effects of localization on the statistics of fluctuations or the random nature of the S-matrix in the various regimes are not addressed here and are deferred to future work.

In section 2 the classical model is described and a kinetic description of classical transport is derived. In sections 3 and 4 we outline the quantum scattering theory for the model, that relies on a Lippmann–Schwinger equation for quantum maps that is derived by paraphrasing standard methods of continuous-time scattering theory; this procedure appears to be generalizable to any scattering model in which the interacting and the free dynamics are defined by discrete unitary groups. In section 5 we describe our numerical method; results are presented in sections 6 and 7, and the concluding section 8 is devoted to further developments. A number of technical details are supplied in the appendixes.

2. The classical model

The classical version of our model is a dynamical system on the cylinder $\Gamma = \{(n, \theta) : -\infty < n < +\infty,\ 0 \leqslant \theta < 2\pi\}$. The discrete time dynamics of this system is specified by a map $\mathcal{F} : \Gamma \to \Gamma$ that carries states $\sigma = (n, \theta)$ into states $\overline{\sigma} = \mathcal{F}\sigma = (\overline{n}, \overline{\theta})$. The explicit form of this map is

$$\begin{aligned} &\overline{n} = n + k \sin \theta \\ &\overline{\theta} = \theta + \tau \overline{n} \qquad \text{for } n_0 \leqslant n \leqslant n_0 + L \\ &\overline{\theta} = \theta \qquad \text{elsewhere} \end{aligned} \tag{1}$$

with k, τ, n_0, L fixed parameters. This map is a modification of the 'free' dynamics $\mathcal{F}_0$ that is formally obtained from (1) by taking $\tau = 0$. As a matter of fact, outside the 'scattering region' $\mathcal{M}$ defined by $n_0 \leqslant n \leqslant n_0 + L$, $\mathcal{F}$ is the same as $\mathcal{F}_0$ and describes a motion with constant speed along straight lines $\theta =$ constant. Inside the scatterer $\mathcal{M}$ points move according to the standard map until they exit, in which case they escape to infinity.

The 'classical scattering matrix' is a map $S : \Sigma_{in} \to \Sigma_{out}$, where $\Sigma_{in,out}$ are the set of admissible incoming (outgoing) states. If $\overline{\sigma} = S\sigma$ then there is a scattering state (i.e. a state which is asymptotically free in the past and in the future) whose orbit is asymptotic to the free orbit of σ in the past and to the free orbit of $\overline{\sigma}$ in the future.

In principle the scattering map can be numerically investigated. However, in the presence of hyperbolicity inside the scattering region (a situation which occurs for $k\tau \gg 1$), the complements of the sets $\Sigma_{in,out}$ will have a complicated fractal geometry (Jung and Scholz 1988, Smilansky 1990). In spite of their negligibly small measure, the exceptional sets will dramatically affect the structure of the scattering map. As a matter of fact, the existence of a fractal set of singularities for the S or related maps has been proposed as the very definition of classical irregular scattering (Jung and Scholz 1988).

Such a 'microscopic' analysis of the present model hardly appears feasible in the case of strong classical chaos ($k\tau \gg 1$) with $L \gg k$, when the standard map dynamics is known to produce diffusive transport. However, a different, 'kinetic' approach proves useful in that case. If $L \gg k$ typical orbits dwell a long time inside the scatterer, much longer than the characteristic time of instability. They therefore experience a large number of almost uncorrelated kicks and a random-walk description proves applicable. In particular, the evolution of an ensemble of orbits distributed in n according to a (suitably smooth) density $f(n)$ with completely random phases obeys the diffusion equation (Lichtenberg and Lieberman 1983)

$$\frac{\partial f(n)}{\partial \tau} = \frac{D}{2}\frac{\partial^2 f(n)}{\partial n^2} \tag{2}$$

where τ is time measured in number of iterates of the map and the diffusion coefficient D is given by†

$$D = \beta\frac{k^2}{2} \equiv \beta D_0 \tag{3}$$

with β a numerical coefficient that depends on the chaos parameter (Rechester *et al* 1981) $K = k\tau$. We can derive a kinetic description of the scattering process by using equation (2) supplemented by boundary conditions at $n = n_0$ and $n = n_0 + L$. The latter conditions result from a trivial balance of the fluxes at the left and right boundaries of $\mathcal{M}$:

$$\begin{aligned} -\frac{D}{2}f'(n_0) &= \Phi_L^{(i)} - \Phi_L^{(o)} \\ -\frac{D}{2}f'(n_0 + L) &= -\Phi_R^{(i)} + \Phi_R^{(o)} \end{aligned} \tag{4}$$

where on the right-hand side the incoming and outgoing fluxes from the left and the right appear, and primes denote derivatives with respect to n. The outgoing flux can be estimated from map (1) by computing the population that is carried out of $\mathcal{M}$ under one iterate of the map. Under the assumption that in neighbourhoods of size

† D_0 is the so-called quasi-linear diffusion coefficient.

k on the left and right boundary f is a linear function of n one obtains

$$\Phi_{\mathrm{L}}^{(\mathrm{o})} = \frac{k}{\pi} f(n_0) + \frac{D_0}{4} f'(n_0)$$
$$\Phi_{\mathrm{R}}^{(\mathrm{o})} = \frac{k}{\pi} f(n_0 + L) - \frac{D_0}{4} f'(n_0 + L). \tag{5}$$

We now assume the incoming fluxes $\Phi_{\mathrm{R,L}}^{(\mathrm{i})}$ to be some known functions of time. Then equations (2), (4) and (5) define an inhomogeneous boundary-value problem that can be solved to find the outgoing fluxes in terms of the incoming ones. Here we give the solution, deferring to appendix D for more details:

$$\begin{vmatrix} \Phi_{\mathrm{R}}^{(\mathrm{o})}(\tau) \\ \Phi_{\mathrm{L}}^{(\mathrm{o})}(\tau) \end{vmatrix} = \int_0^\infty \mathrm{d}\sigma \begin{vmatrix} \mathcal{G}_1(\sigma) - \delta(\sigma) & \mathcal{G}_2(\sigma) \\ \mathcal{G}_2(\sigma) & \mathcal{G}_1(\sigma) - \delta(\sigma) \end{vmatrix} \begin{vmatrix} \Phi_{\mathrm{R}}^{(\mathrm{i})}(\tau - \sigma) \\ \Phi_{\mathrm{L}}^{(\mathrm{i})}(\tau - \sigma) \end{vmatrix}. \tag{6}$$

The 'memory kernels' $\mathcal{G}_{1,2}$ in equation (6) are given by

$$\mathcal{G}_j(\sigma) = \sum_{n=1}^{\infty} \lambda_n \mathrm{e}^{-\lambda_n \sigma} x_{n,j} \qquad j = 1, 2. \tag{7}$$

The coefficients $x_{n,j}$ are given in appendix D. The numbers λ_n in these formulae are the eigenvalues of the homogeneous problem. They give the spectrum of diffusive decay rates and are given by

$$\lambda_n = \frac{2D}{L^2} \nu_n^2 \tag{8}$$

where the numbers ν_n are obtained by arranging the roots of the equations into an increasing sequence

$$\tan(\nu) = \begin{cases} a/\nu \\ -\nu/a \end{cases} \qquad a = \frac{2kL}{\pi \tilde{D}} \qquad \tilde{D} \equiv D_0(2\beta - 1). \tag{9}$$

It goes without saying that this is just an approximate description of the actual scattering process associated with map (1). A smoothing in time and in n as well is implicit in the derivation of the diffusion equation. Besides washing out the intricated phase space structures that characterize the microscopic dynamics, this process introduces arbitrarily fine scales of its own, that are associated with the unbounded sequence of eigenvalues of the diffusion problem. Some cutoff must therefore be understood for the sum (7).

If the incoming flux is stationary then (6) yields

$$\begin{vmatrix} \Phi_{\mathrm{R}}^{(\mathrm{o})} \\ \Phi_{\mathrm{L}}^{(\mathrm{o})} \end{vmatrix} = \begin{vmatrix} 1 - \eta & \eta \\ \eta & 1 - \eta \end{vmatrix} \begin{vmatrix} \Phi_{\mathrm{R}}^{(\mathrm{i})} \\ \Phi_{\mathrm{L}}^{(\mathrm{i})} \end{vmatrix}. \tag{10}$$

The transmission coefficient η is

$$\eta = \frac{\pi D}{\pi \tilde{D} + 2kL}. \tag{11}$$

For large L, η is therefore inversely proportional to L (Ohm's law). Direct numerical computations of the transmission coefficient from the microscopic dynamics (1) confirm the law (11) at large L (figure 1); at small values $L \sim k$ this formulation is meaningless.

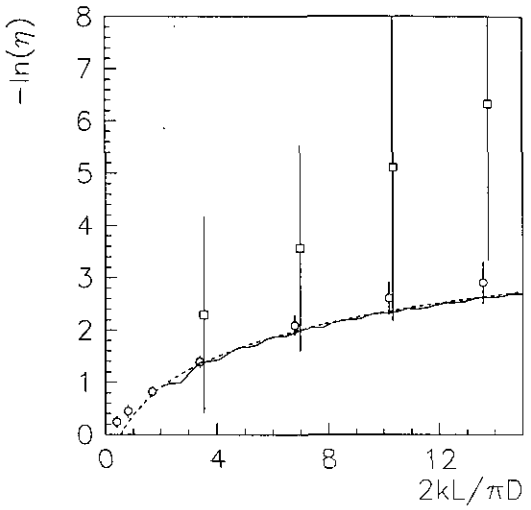

Figure 1. Logarithm of the inverse transmission coefficient against the scaled length $2kL/\pi D$ of the sample. Quantum data from averages 50–200 different samples. Circles, $q = 29, \xi = 1, 2\xi q\tau = 10$; squares, $q = 29, \xi = 0.1, 2\xi q\tau = 10$. The broken curve is the classical theoretical prediction, equation (11); the full curve, classical numerical prediction.

3. The quantum model

Time-dependent models such as the KR involve inelastic scattering. Nevertheless the mathematical apparatus of elastic scattering theory can still be implemented by resorting to the quasi-energy formalism. The latter is especially simple when the one-cycle unitary propagator is explicitly known, and this is just the case with the KR model, the quantum dynamics of which is defined in the Hilbert space $L^2(0, 2\pi)$ by the unitary operator

$$U = TU_0. \tag{12}$$

Here U_0 is multiplication by $\exp(\mathrm{i}V(\theta))$ and describes the effect of one kick; although we have in mind the KR, for which $V(\theta) = k\cos\theta$, the real function $V(\theta)$ will be left unspecified for the time being. We shall assume here $\hbar = 1$; as is well known, the classical limit is then approached by letting $k \to \infty, \tau \to 0, k\tau =$ constant. The operator T describes a free rotation occurring between subsequent kicks. Unlike the conventional KR, T will be different from the identity only in that subspace in which the momentum n takes values inside the scatterer $\mathcal{M}$: $n_0 \leqslant n \leqslant n_0 + L$. Therefore T will be given by

$$T = \sum_{n\in\mathcal{M}} \mathrm{e}^{-\mathrm{i}n^2\tau/2}|n\rangle\langle n| + \sum_{n\in\mathbb{Z}\setminus\mathcal{M}} |n\rangle\langle n| \tag{13}$$

where

$$|n\rangle = (2\pi)^{-1/2}\mathrm{e}^{\mathrm{i}n\theta} \tag{14}$$

are the momentum eigenstates. The discrete-time dynamics generated by the operator U can be viewed as a perturbation of the free dynamics generated by the operator

U_0 (in other words, contrary to what is usually done, here we are considering the 'rotation' as a perturbation of the 'kick'). A convenient picture is gained by going over to the momentum representation, in which wavepackets propagate on the discrete one-dimensional lattice labelled by the integer values n of quantized momentum. The free dynamics is ballistic with the expectation value of $|n|$ growing linearly in time and the spectrum of the operator U_0 is purely absolutely continuous. The quasi-energy (QE) spectrum (denoted by Spec in the following) is the set of the eigenphases $\lambda \in [0, 2\pi]$; it coincides with the range of the function $V(\theta)(\mathrm{mod} 2\pi)$. For any QE $\lambda \in \mathrm{Spec}$ the equation

$$\lambda = V(\theta) \pmod{2\pi} \tag{15}$$

has a finite number N_λ of real roots θ_α, $\alpha = 1, 2, \ldots, N_\lambda$. Every such root has associated with it a free QE eigenfunction $u_0^{\lambda,\alpha}$ which in the coordinate representation has the form

$$\langle \theta | u_0^{\lambda,\alpha} \rangle = \delta(\theta - \theta_\alpha) \tag{16}$$

but in the momentum representation its form is

$$\langle n | u_0^{\lambda,\alpha} \rangle = (2\pi)^{-1/2} \mathrm{e}^{-\mathrm{i}n\theta_\alpha}. \tag{17}$$

In the lattice picture, these eigenfunctions describe plane waves with wavenumbers θ_α. For any given λ, the set of such wavenumbers or 'channels', is the *QE shell* at the QE λ. If the QE shell at λ consists of N_λ wavenumbers, then the QE eigenvalue λ is N_λ times degenerate. For $V(\theta) = k \cos\theta$ and large k one has $N_\lambda \sim 2\pi^{-1}k$ i.e. N_λ is of the order of the number of states effectively coupled by one kick. Moreover, the channels come in pairs $\theta_\alpha, \theta_{\alpha^*}$ with opposite velocities: $\theta_\alpha + \theta_{\alpha^*} = 2\pi$.

The QE shells define a fibration of the Hilbert space into N_λ-dimensional fibres. In fact any wavefunction can be expanded in the form:

$$\psi(n) = \int_{\mathrm{Spec}} \mathrm{d}\lambda \sum_\alpha x_\alpha(\lambda) |\nu_\alpha| u_0^{\lambda,\alpha}(n) \tag{18}$$

where ν_α is

$$\nu_\alpha = \left(\frac{\mathrm{d}V}{\mathrm{d}\theta} \right)^{-1}_{\theta=\theta_\alpha} \tag{19}$$

and $|\nu_\alpha|$ is the density of states. The N_λ-dimensional complex vector with components $x_\alpha(\lambda)$ is a fibre of the wavefunction at the QE λ. Its squared norm gives the total flux of free waves with QE λ (see also later) and is given by

$$\sum_{\alpha=1}^{N_\lambda} |\nu_\alpha| |x_\alpha(\lambda)|^2. \tag{20}$$

The conservation of QE has no classical counterpart. It reflects the fact that the scattering process changes the free energy by an integer number of quanta. With

the present choice of units, one quantum of QE is just 2π and a condition for quasi-classicity is therefore $k \gg 2\pi$, consistently with a previous remark.

The dynamics (12) has no other symmetry, in particular it is not time-reversal invariant†.

The complete dynamics (12) describes wavepackets that come in from infinity, and enter the interaction region $\mathcal{M}$, whence they are partly reflected and partly transmitted. A complete description of this scattering process is provided by the scattering operator, that can be constructed as shown in the next section.

4. The Lippmann–Schwinger equation and the S-matrix

Due to the conservation of QE, the scattering operator preserves the previously described fibration and is therefore a fibred operator itself. In other words, it is specified by a unitary matrix-valued function $S_{\alpha\beta}(\lambda)$ $(\alpha, \beta = 1, 2, \ldots, N_\lambda)$ that determines the asymptotics of interacting QE eigenfunctions at large distance from the scatterer in the form:

$$u^\lambda(n) \sim \sum_{\alpha=1}^{N_\lambda} a_\alpha(\lambda) u_{0,\mathrm{in}}^{\lambda,\alpha}(n) + \sum_{\alpha,\beta=1}^{N_\lambda} |\nu_\alpha|^{1/2} |\nu_\beta|^{-1/2} S_{\alpha\beta}(\lambda) a_\beta(\lambda) u_{0,\mathrm{out}}^{\lambda,\beta}(n) \qquad (21)$$

where the suffix 'in' (respectively, 'out') of a free plane wave means that that particular wave does, in fact, appear in the sum only if, in the considered region (either far to the left or far to the right of the scatterer), it is incoming (respectively, outgoing), and a_α are arbitrary complex amplitudes. The asymptotic form (21) is approached exponentially fast on moving away from the scatterer; in practice, it is valid at distances larger than $\sim k$ from the scatterer.

The scattering operator can be constructed by a more or less straightforward adaptation of standard methods from continuous-time scattering theory. Eigenfunctions of the complete propagator (12) in the form of distorted plane waves are obtained by solving an equation of the Lippmann–Schwinger type; this equation is derived in appendix A by paraphrasing methods of conventional scattering theory (Prugovechky 1971) and has the form:

$$u_+^{\lambda,\alpha} - \mathrm{e}^{\mathrm{i}\lambda} G_+(\lambda)(T^\dagger - 1) u_+^{\lambda,\alpha} = u_0^{\lambda,\alpha} \qquad (22)$$

where $u_+^{\lambda,\alpha}$ is the sought for 'interacting' eigenfunction associated with the 'free' eigenfunction $u_0^{\lambda,\alpha}$, and

$$G_+(\lambda) = \lim_{\epsilon \to 0+} (U_0 - \mathrm{e}^{\mathrm{i}\lambda + \epsilon})^{-1}. \qquad (23)$$

The scattering matrix $S(\lambda)$ is given in terms of the distorted plane waves u_+ by the following equation, which is justified in appendix B:

$$S_{\alpha\beta}(\lambda) = \delta_{\alpha\beta} - H_{\alpha\beta} |\nu_\beta|^{1/2} |\nu_\alpha|^{1/2} \qquad (24)$$

† The complete KR is known to have some symmetries of its own, but these symmetries are generically destroyed upon restricting the dynamics to a finite region $\mathcal{M}$.

where $\alpha, \beta = 1, 2, \ldots, N_\lambda$ and

$$H_{\alpha\beta} = 2\pi\langle (T-1)u_0^{\lambda,\alpha} | u_+^{\lambda,\beta}\rangle. \tag{25}$$

Since $T-1$ is different from zero only at a finite number $L+1$ of sites in $\mathcal{M}$, only a finite string of $L+1$ values of the eigenfunction u_+ at sites inside $\mathcal{M}$ is needed in order to compute $S_{\alpha\beta}$. On multiplying equation (22) on the left by $\langle n|$, $n_0 \leqslant n \leqslant n_0 + L$ these values of u_+ are found to satisfy a set of $L+1$ linear equations:

$$\sum_{k=n_0}^{n_0+L} \left[\delta_{nk} - \mathrm{e}^{\mathrm{i}\lambda} G^+_{n-k}(T_k^* - 1)\right] u_+(k) = (2\pi)^{-1/2}\mathrm{e}^{-\mathrm{i}n\theta_\alpha} \qquad n = n_0, \ldots, n_0 + L \tag{26}$$

(superscripts in u_+ have been dropped for simplicity). G_n^+ are the Fourier coefficients of the *free Green function*:

$$G_n^+ = (2\pi)^{-1/2}\langle n|G_+(\lambda)|0\rangle = (2\pi)^{-1} \lim_{\epsilon\to 0+} \int_0^{2\pi} \frac{\mathrm{e}^{-\mathrm{i}n\theta}\,\mathrm{d}\theta}{\mathrm{e}^{\mathrm{i}V(\theta)} - \mathrm{e}^{\mathrm{i}\lambda+\epsilon}}. \tag{27}$$

In spite of the absence of symmetries in the interacting dynamics, the S-matrix has one important symmetry expressed by the reciprocity property:

$$S_{\alpha\beta} = S_{\beta^*\alpha^*}. \tag{28}$$

As shown in appendix C this property stems from the time-reversal invariance of the free dynamics.

The S-matrix establishes a connection between incoming and outgoing fluxes, as follows. Consider a 'quasi-classical' free wavefunction:

$$\psi(n,t) = \int_{\mathrm{Spec}} \mathrm{d}\lambda \sum_\alpha x_\alpha(\lambda)|\nu_\alpha|\mathrm{e}^{-\mathrm{i}\theta_\alpha(\lambda)n + \mathrm{i}\lambda t} \tag{29}$$

with a narrow spread in λ around some average value λ_0. The flux at site n 'in the α-channel' is (after averaging over approximately k sites; here and in the following the specification of the integration domain will be omitted):

$$\Phi(n,t) \sim |\nu_\alpha| \int x_\alpha(\lambda)\overline{x}_\alpha(\lambda')\mathrm{e}^{\mathrm{i}(\lambda-\lambda')(t-\nu_\alpha n)}\,\mathrm{d}\lambda\,\mathrm{d}\lambda' \tag{30}$$

where ν_α is taken at $\lambda = \lambda_0$. The Fourier transform in time of this flux is

$$\hat{\Phi}(n,\omega) \sim |\nu_\alpha|\mathrm{e}^{-\mathrm{i}\nu_\alpha n\omega} \int \overline{x}_\alpha(\lambda)x_\alpha(\lambda+\omega)\,\mathrm{d}\lambda. \tag{31}$$

Since time is a discrete variable in this model, ω takes values in $[0, 2\pi]$. Suppose that the wavefunction incoming from the left ($n \ll n_0$) is a free wave in the β-channel. The (Fourier transform of) the outgoing reflected flux in an outgoing channel α (that

will be taken to the left, too, in order to fix ideas) will be, from equations (21), (30) and (31):

$$\overline{\hat{\Phi}}^{\alpha}_{\mathrm{out}}(n,\omega) \sim \mathrm{e}^{-\mathrm{i}(\nu_\alpha-\nu_\beta)\omega n}\mathcal{C}_{\alpha\beta}(\lambda_0,\omega)\overline{\hat{\Phi}}^{\beta}_{\mathrm{in}}(n,\omega) \tag{32}$$

with

$$\mathcal{C}_{\alpha\beta}(\lambda_0,\omega) = \overline{S_{\alpha\beta}(\lambda_0)S_{\alpha\beta}(\lambda_0+\omega)}. \tag{33}$$

The upper bars in (32) and (33), denote some kind of averaging, either over 'disorder' (as we shall assume) or over a number of channels that, although large, corresponds to but a small classical spread in velocity. It is assumed that the resulting autocorrelation $\mathcal{C}$ will be slowly varying with λ. The phase of the exponential factor is

$$\omega t^{(\mathrm{f})}_{\alpha\beta} = (\nu_\alpha - \nu_\beta)n\omega \tag{34}$$

with $t^{(\mathrm{f})}$ the time of free flight through the scattering region. Therefore, the right-hand side of equation (32) is the Fourier transform of the incoming free flux shifted in time so as to account for the time of free flight. Equations (32) and (34) show that outgoing fluxes are connected to incoming fluxes by an integral transform that we write in a sketchy symbolic way as

$$\overline{\Phi}_{\mathrm{out}}(t) = \int_0^\infty \check{\mathcal{C}}(\sigma)\overline{\Phi}_{\mathrm{in}}(t-\sigma-t^{(\mathrm{f})})\,\mathrm{d}\sigma. \tag{35}$$

The 'response kernel' of this transform is the inverse Fourier transform of the autocorrelation of the scattering matrix. This kernel has support in the positive real axis due to the causal property of the scattering matrix, which in turn relies on the S-matrix being the boundary value on the unit circle of a function analytic in the exterior of the circle.

5. Numerical procedures

The core of our numerical method is the solution of equation (26) that calls for numerically inverting a matrix of rank $L+1$ which is constructed by means of the Fourier coefficients of the Green function. Once these coefficients are known, equations (26) can be easily solved numerically, but the very computation of these coefficients is the crux of the matter, because the unitarity of the S-matrix is quite sensitive to their accuracy (unitarity of the S-matrix is not built-in in our method and therefore provides a good check for the accuracy of the simulations). A direct numerical computation with $V(\theta) = k\cos\theta$ proved very difficult and unreliable, and we had to resort to a different approximation. We chose

$$\begin{aligned} V(\theta) &= \frac{1}{\mathrm{i}}\ln\left(\frac{1-\mathrm{i}\xi\cos\theta}{1+\mathrm{i}\xi\cos\theta}\right)^q \\ &= 2q\arctan(\xi\cos\theta) \end{aligned} \tag{36}$$

with q an integer. In the limit $\xi \to 0, q \to \infty, 2\xi q \to k$ this yields $V(\theta) = k\cos\theta$ and the map defined by the potential (36) for small ξ and large q therefore provides a smooth approximation for the KR; we shall comment further on this point in section 6. Needless to say, the model thus obtained (referred to as 'the arctan model' in the following) can also be studied in its own right. With this choice of V, the integral in equation (27) can be turned into the integral of a *rational* function along the unit circle in the complex plane, that could be computed by means of a computer-assisted summation of residues. In most of the computations reported in this paper the lack of unitarity, as measured by the deviation of the eigenvalues of the S-matrix from the unit circle, was of order 10^{-6} or less.

6. Transport and localization

Both the classical KR and its approximation, the classical arctan model, exhibit diffusion in the deeply chaotic regime and the classical transmission coefficient is found to obey an ohmic law as a function of the sample size, as shown in figure 1.

In contrast to this classical behaviour, the quantum models exhibit localization. In the limit case of an infinitely long scatterer, wavepackets initially concentrated at some site $\overline{n}$ inside it do not spread indefinitely in the course of their evolution, but eventually enter an oscillatory regime, in which the average population of the sites decreases exponentially away from the initial site. The scatterer behaves like a 'sample' of a disordered solid; the finite string of 'pseudorandom' complex numbers T_k, $(n_0 \leqslant k \leqslant n_0 + L)$ plays the same role as that of the random potential in tight-binding models. If n_0 is changed a different string is obtained, i.e. a different realization of the pseudorandom potential; therefore averaging over different choices of n_0 is equivalent to averaging over disorder in tight-binding models.

In the quasi-classical regime (i.e. for $2\xi q \gg 1, \tau \ll 1$), the localization length l for the infinite sample is approximately equal to the classical diffusion coefficient. This theoretical prediction (Shepelyansky 1986) is confirmed for the arctan model by our data in figure (2) where numerically obtained diffusion coefficients are compared with localization lengths from a numerical simulation of the quantum evolution inside a very long sample. In the same figure 2 the classical diffusion coefficient as given by formula (3) for the KR is also shown, thus illustrating the extent to which the arctan model approximates the KR (for the value of the stochasticity parameter chosen for figure 2 one has $\beta \approx 0.647$) (Rechester *et al* 1981).

The transmission coefficient is defined as the sum of the squared moduli of all the S-matrix elements for transitions between free states with the same direction of propagation, divided by N_λ. The dependence of the quantum transmission coefficient η of the arctan model on the size of the sample is illustrated in figure 1, where the average of the logarithm of $1/\eta$ over 50–100 realizations is plotted against the scaled length of the sample: two sets of quantum data corresponding to different values of l are shown. Besides l, one more parameter determines the structure of figure 1, and this is k, that sets the scale of the mean free path because it gives the (order of) the distance travelled between subsequent 'collisions' ('collisions' are described by the operator T, so the mean free path is the number of states coupled by the operator U_0). The scaled length on the horizontal axis is approximately the same as length measured in units of this mean free path. With this scaling the same theoretical

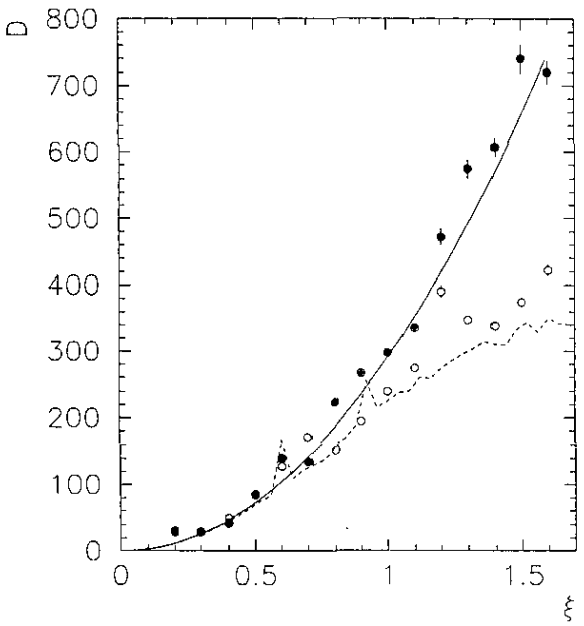

Figure 2. Localization length (open circles) and classical diffusion coefficient (broken curve) for the quantum arctan model as a function of ξ for fixed $q = 15$ and $2\xi q\tau = 10$ (open circles). The full circles give localization lengths for the KR with $k = 2\xi q$. The classical diffusion coefficient $D = k^2\beta/2$ for the KR is also shown (full curve).

classical behaviour (broken curve) would be predicted by the Fokker–Planck model, see equation (11)†.

The left-hand part of figure 1 corresponds to the 'ballistic' regime, where the length is less than or of the order of the mean free path. The right-hand part, where $L > l$, corresponds to the 'localized', insulator regime, marked by an exponential increase in the resistance with the length and by large relative fluctuations of the transmission coefficient. Obtaining more data farther to the right is difficult because the transmission coefficient rapidly falls to the level of the numerical unitarity defect.

The crossover between the ballistic and insulator regimes occurs in a range of lengths roughly defined by $k < L < l$. This range becomes larger, the larger k, as is seen by comparing the two sets of quantum data in figure 1. The reason is that $l \sim k^2/2$: circles in figure 1 have a (numerical) localization length $l \sim 880$ and the last circle to the right corresponds to a sample length $L = 400$; squares have a localization length $l \sim 26$. Thus as k and L increase at fixed k/L (i.e. going towards the classical limit) the model tends to behave like an ohmic conductor, and the ballistic range becomes negligible in comparison with the ohmic range. This marks a distinct difference between this model and quasi-one-dimensional models of the Anderson type, where the mean free path is proportional to l. An interesting remark connected with this fact is that the ohmic law (11) *does not* scale with the ratio l/L; the reason is that the number of channels is not fixed but is itself proportional to the mean free path.

† Provided that $k\tau$ is kept constant.

7. Fluctuations

Ericson fluctuations of nuclear cross sections against energy are expected to appear when the excitation is so strong that many scattering resonances strongly overlap, and the energy scale of the fluctuations should be defined by the resonance width (Brody *et al* 1981). Fluctuations of the same statistical nature as Ericson's are also expected for quantum cross sections of classically chaotic scattering processes; here, too, the S-matrix elements are expected to fluctuate with energy in the regime of overlapping resonances, on a scale semiclassically defined by the classical decay rate, or inverse time of escape (Smilansky 1990).

Fluctuations of S-matrix elements could be easily observed in our model. In figure 3 we show the squared modulus of a scattering matrix element (a reflection one) against the 'control' parameter ξ for a ballistic case with scaled length ~ 2 (changing the value of ξ directly affects the value of the QE; also recall that changing ξ is tantamount as changing k in the KR). For the sake of comparison, the same plot is shown in the integrable case, where it displays much more regular behaviour.

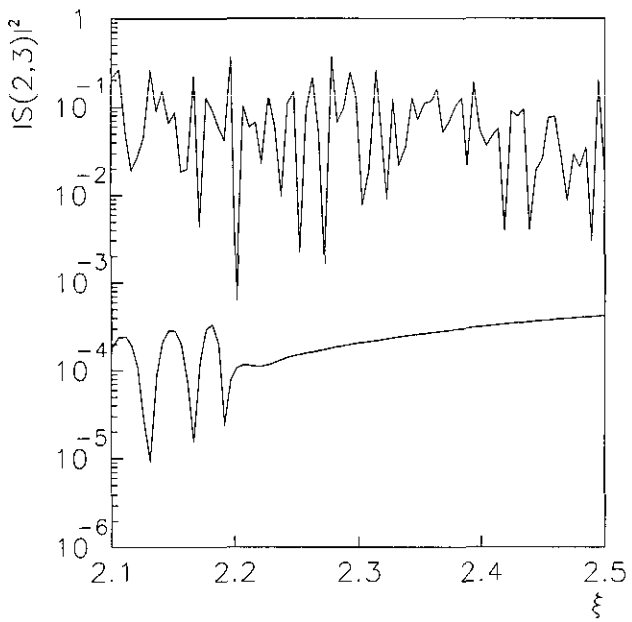

Figure 3. Fluctuations of a reflection cross section on changing ξ, for $q = 15$, $2\xi q\tau = 0.05$ (lower curve, integrable case) and for $2\xi q\tau = 10$ (upper curve, chaotic case). The sample size was $L = 100$.

Similar fluctuations were observed for the matrix elements as functions of QE. Figure 4 shows how phase shifts change with the QE in a small neighbourhood of $\lambda = 0$, the size of which is of the order of the correlation length for the same data (see later).

Ericson fluctuations have two distinctive marks. First, the S-matrix at given energy should look like a random matrix picked from an appropriate ensemble; second, correlations of S-matrix elements at different energies should have a Lorentzian dependence on the energy spacing. The first aspect will not be addressed here, except for the somewhat trivial remark that traditional ensembles such as Dyson's

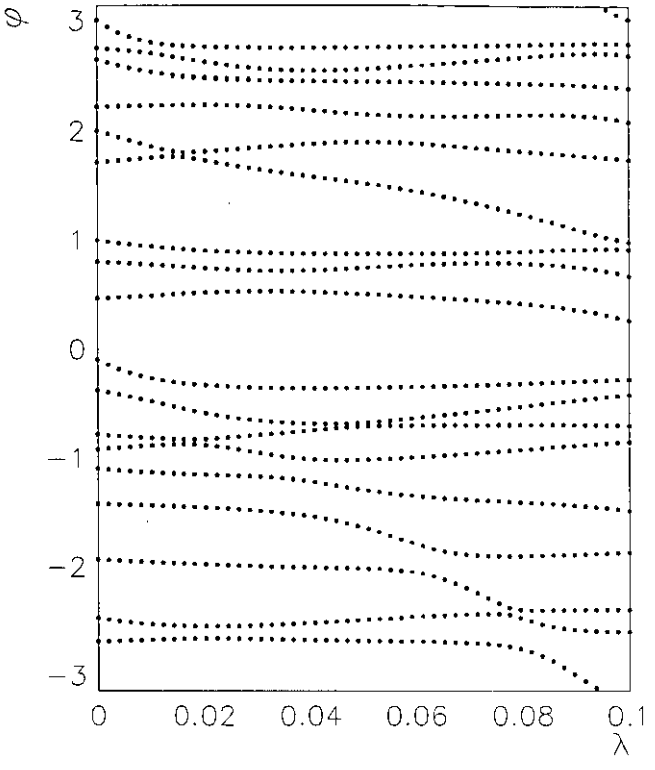

Figure 4. Phase shifts φ against QE λ at $q = 15, \xi = 1.5, 2\xi q\tau = 10, L = 200$ (same data as for figure 6).

circular ensembles or the like cannot be expected to do this job; in the diffusive regime, the S-matrix is by no means (statistically) invariant under rotations, because the transmission and reflection submatrices have different magnitudes, so that more sophisticated ensembles will have to be used as a term of comparison. As to the second aspect we computed, following Smilansky (1990), the function $C_{\alpha\beta}(\omega)$ defined by

$$C_{\alpha\beta}(\lambda,\omega) = \frac{|\mathcal{C}_{\alpha\beta}(\lambda,\omega)|^2}{|\mathcal{C}_{\alpha\beta}(\lambda,0)|^2} \tag{37}$$

with $\mathcal{C}_{\alpha\beta}$ as in equation (33), by averaging over 50–100 different samples with the same size and different n_0. The reference value λ was taken 0 ('band centre'). In the ballistic and close to ballistic cases, smooth bell-shaped curves were typically found. In many cases, a Lorentzian fit proved very good over a large interval; in other cases, relevant deviations from Lorentzian were found only in the tails; finally, in a minority of cases deviations were found both at small and at large values of ω (interestingly, such deviant results were mostly obtained with transmission rather than reflection matrix elements: the reason is still not clear to us). Figures 5(*a*)–(*d*) show typical results.

According to equation (35), the inverse Fourier transforms of the autocorrelation of the S-matrix elements play the role of memory kernels relating outgoing fluxes to incoming ones. Since the corresponding classical kernels exponentially decay with

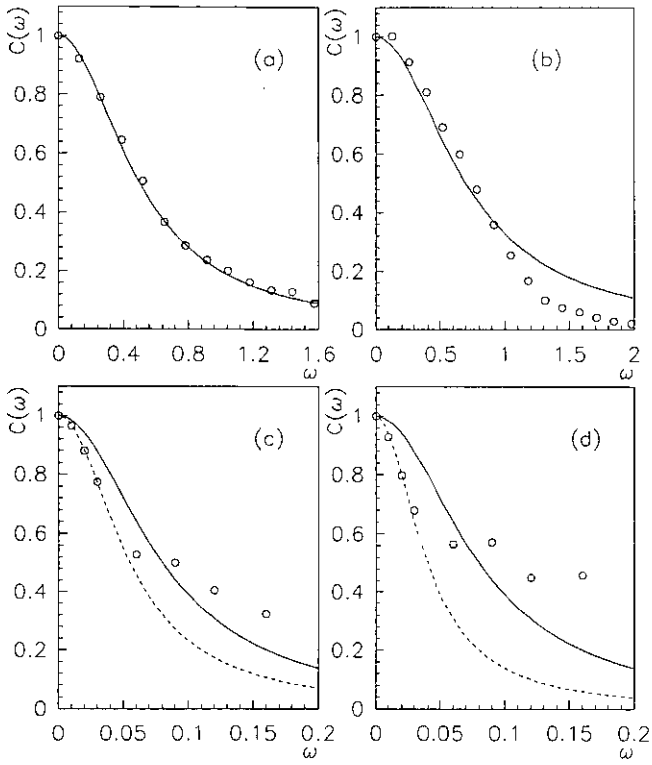

Figure 5. Squared moduli of some normalized QE autocorrelations of different S-matrix elements (equation (37)) averaged over 100 different samples, for $\lambda = 0$ (band centre) $2\xi q\tau = 10, \xi = 1.5, q = 15$: (*a*), $L = 50$; (*b*), $L = 28$; (*c*) and (*d*), $L = 200$ (two different matrix elements). Full curves are Lorentz curves of width corresponding to the average correlation length of six different S-matrix elements. The broken curves are Lorentz curves fitting the first four data.

time, as shown in section 2, one may expect that under suitable semiclassical conditions the quantum kernels will also decay exponentially, possibly after some initial non-universal stage; this expectation is also substantiated by general arguments relying on semiclassical formulae for the scattering matrix (Smilansky 1990). Thus the behaviour of $C_{\alpha\beta}(\omega)$ for not too large ω should be Lorentz-like, as indeed we observed; moreover, the width of the Lorentz curve should be given by the classical rate of exponential decay. In figure 6 classical decay rates and quantum correlation lengths for the arctan model are plotted against the variable l/L^2. The latter variable is roughly proportional to the square of the inverse scaled length; it is small in the diffusive regime and in that case it is roughly proportional to the classical diffusive decay rate (the theoretical diffusive decay rate, as given by the lowest eigenvalue of the diffusion equation, equation (9), is shown by the full curve in figure 6). Correlation lengths were determined as the values of ω at which $C_{\alpha\beta}$ was found to decay to a value 0.5; the data in figure 6 were obtained by averaging the correlation lengths of six different S-matrix elements. The right-hand part of figure 6 corresponds to the ballistic regime; there, classical rates and quantum correlations lengths exhibit fairly good agreement.

Going towards the left in figure 6 one classically approaches the diffusive regime. Since l was kept constant in these computations, quantum mechanically one ap-

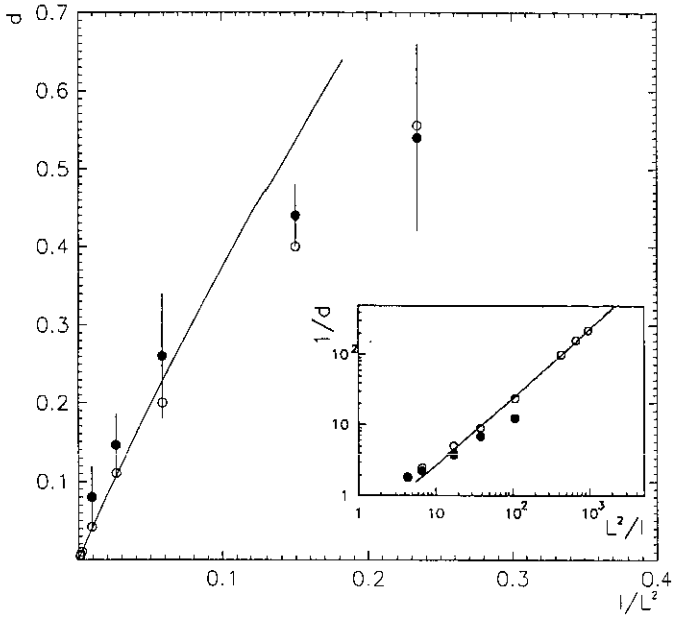

Figure 6. Quantum correlation lengths (full circles) and numerically computed classical decay rates (open circles) against the ratio l/L^2 for $q = 15, \xi = 1.5, 2\xi q\tau = 10$. Quantum data are obtained by averaging the correlation lengths of six different S-matrix elements. A bilogarithmic plot is shown in the insert. Full lines give the classical decay rates as predicted by the Fokker–Planck equation.

proaches the localized regime; the quantum data closest to the origin were obtained at $l/L \simeq 3$. A bilogarithmic plot of the left-hand part of figure 2 yields a clear indication that quantum correlation lengths decrease more slowly than classical decay rates and tend, therefore, to be significantly higher. The 'Lorentzian range' of the corresponding correlation curves becomes very narrow around $\omega = 0$ and, in general, these curves develop a very slowly decaying tail. The width of the Lorentzian curve that fits the correlation curve near $\omega = 0$ is significantly smaller than the global correlation length (figures 5(*c*) and (*d*)).

Thus our data indicate that the statistical properties of the S-matrix fluctuations undergo a qualitative change on moving from the ballistic regime towards the diffusive one. Generally speaking, Ericson fluctuations are expected to be Lorentz-correlated when the resonances have roughly the same width; therefore the observed behaviour may be a symptom that the distribution of the resonance widths is becoming broader in the diffusive regime.

A remarkable feature of the fluctuations in the quantum ohmic regime emerges when their magnitude is investigated as a function of the sample length. In figure 7 we show a plot of the variance $\delta\eta$ of the transmission coefficient η against the scaled length. These variances were obtained by either choosing different samples with the same values of ξ, q, τ and QE λ or slightly varying some of the latter parameters around the values previously used for the weakly localized case in figure 1, at fixed disorder.

On comparing figures 7 and 1 one sees that in the ohmic regime the fluctuations have approximately the same magnitude, no matter how they were generated. This behaviour bears a definite similarity to the universal conductance fluctuations observed

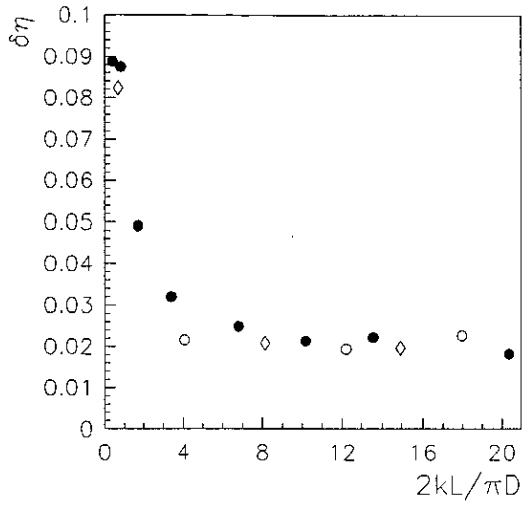

Figure 7. Variance $\delta\eta$ of the quantum transmission coefficient against the scaled length $2kL/\pi D$: full circles, variances over 50 different samples with $q = 21, \xi = 1, 2q\xi\tau = 10$, OE $\lambda = 0$; open circles, variances over 30 different values of λ in a range of 10 correlations lengths around $\lambda = 0, q, \xi, \tau$ as above, fixed sample; lozenges, variances over 5–10 different values of ξ in a range 1 ± 0.025 with a fixed sample and constant $q = 29, 2q\xi\tau = 10$.

in mesoscopic devices. In our range of length the relative fluctuations $\delta\eta/\eta$ changed from ~ 0.1 to ~ 0.5.

8. Concluding remarks

The effect of quantization on classical chaotic transport is a widely studied subject, as is the nature of quantum scattering in the presence of classical chaos. Nevertheless, problems exhibiting both features at one time, i.e. scattering problems in which chaotic diffusion occurs inside the interaction region have scarcely been studied up to now (Borgonovi *et al* 1981), mainly because realistic models involve great computational difficulties. On the other hand, scattering problems of this sort have a broad physical relevance. In this paper we have described a model for 'diffusive scattering' that can be effectively analysed both in its classical and its quantum mechanical version. This was at the price of two major shortcomings. In the first place, the model is a very unphysical one; although we have been comparing it with electronic transport in disordered solids throughout this paper, it is certainly hard to conceive any real physical system described by such a dynamics. Second, our model involves inelastic scattering—although in the quantum case the conservation of QE makes it possible to think of it as describing the elastic scattering of waves with an unusual dispersion law.

In spite of these disadvantages, we believe that the indications provided by our abstract model have some general validity, as was the case for the KR of which our model is a variant.

Two essential features of transport in disordered solids, i.e. diffusion and localization, are represented in this model and we have shown how a quantum ohmic regime stems from the interplay of these competing effects. This demonstrates that classical

chaotic properties can produce statistical behaviour in 'small' quantum systems, in spite of the well known absence of chaos in quantum mechanics. Moreover, the magnitude of transmission fluctuations in the quantum ohmic regime is, according to our data, approximately universal. Our model appears, therefore, to be able to qualitatively reproduce an important feature of real quantum transport.

A major motivation for this work was the analysis of the scattering matrix fluctuations. We have provided evidence that these fluctuations are Ericson-like in the ballistic regime, and that their correlation length can be inferred from knowledge of classical escape rates. The ballistic regime of our model thus provides one more specific instance in support of some general views about quantum irregular scattering (Smilansky 1990).

Many other important questions remain open. The nature of fluctuations in the ohmic and in the localized regime is still unclear: our data indicate that the simple Ericson picture needs to be modified on approaching the classical diffusive regime. A more detailed analysis, including the investigation of poles of the S-matrix, is required and is now in progress.

Acknowledgments

We acknowledge useful discussion with S Fishman and F M Izrailev.

Appendix A: The Lippmann–Schwinger equations

Consider the Moller wave operators

$$\Omega_{\pm} = \lim_{n \to \pm\infty} U^n U_0^{-n}. \tag{A1}$$

Due to their intertwining property, they transform the eigenfunctions of the free dynamics U_0 into eigenfunctions of the interacting dynamics U. In particular, a couple of interacting eigenfunctions $u_{\pm}^{\lambda,\alpha}$ can be formally associated with any free eigenfunction $u_0^{\lambda,\alpha}$ as follows.

$$u_0^{\lambda,\alpha} = \Omega_{\pm}^{-1} u_{\pm}^{\lambda,\alpha} \tag{A2}$$

Upon choosing the + sign and substituting (A1) into (A2) one gets the first Lippmann–Schwinger equation:

$$\begin{aligned} u_0^{\lambda,\alpha} &= \lim_{\epsilon \to 0+} \epsilon \sum_{n=0}^{\infty} \mathrm{e}^{-\epsilon n} U_0^n U^{-n} u_+^{\alpha,\lambda} \\ &= \lim_{\epsilon \to 0+} \left[1 + \sum_{1}^{\infty} \mathrm{e}^{-\epsilon n} U_0^{n-1} (T^{\dagger} - 1) U^{-n+1} \right] u_+^{\lambda,\alpha} \\ &= \lim_{\epsilon \to 0+} \left[1 + \mathrm{e}^{\mathrm{i}\lambda} \sum_{1}^{\infty} \mathrm{e}^{-(\epsilon + \mathrm{i}\lambda)n} U_0^{n-1} (T^{\dagger} - 1) \right] u_+^{\lambda,\alpha} \\ &= \left[1 - \mathrm{e}^{\mathrm{i}\lambda} \lim_{\epsilon \to 0+} (U_0 - \mathrm{e}^{\mathrm{i}\lambda + \epsilon})^{-1} (T^{\dagger} - 1) \right] u_+^{\lambda,\alpha} \end{aligned} \tag{A3}$$

Instead, choosing the − sign in (A2) leads to the second Lippman–Schwinger equation:

$$u_0^{\lambda,\alpha} = \left[1 + \lim_{\epsilon \to 0+} (U_0 - e^{i\lambda - \epsilon})^{-1}(T-1)U_0\right] u_-^{\lambda,\alpha}. \tag{A4}$$

Appendix B: The scattering matrix from distorted plane waves

For integer n define

$$\begin{aligned} \Omega_n &= U^n U_0^{-n} \\ &= UU_0^{-1} + \sum_{k=1}^{n-1} U^k \left[UU_0^{-1} - 1\right] U_0^{-k} \end{aligned} \tag{B1}$$

which for arbitrary states ψ, g and integers $n_1 < n_2$ yields

$$\langle (\Omega_{n_2} - \Omega_{n_1})\psi | g \rangle = \sum_{k=n_1}^{n_2-1} \langle U^k (T-1) U_0^{-k} \psi | g \rangle. \tag{B2}$$

We now let $n_1 \to -\infty, n_2 \to +\infty$. Moreover, we put $g = \Omega_+ \phi$ in (B2) and we use the definition of the scattering operator:

$$S = \Omega_-^\dagger \Omega_+ \tag{B3}$$

and we find

$$\langle \psi | S\phi \rangle = \langle \psi | \phi \rangle - \sum_{k=-\infty}^{+\infty} \langle (T-1) U_0^{-k} \psi | \Omega_+ U_0^{-k} \phi \rangle. \tag{B4}$$

Both ψ and ϕ can be expanded in free plane waves according to

$$\psi = \int_{\text{Spec}} d\lambda \sum_{\alpha=1}^{N_\lambda} u_0^{\lambda,\alpha} |\nu_\alpha| \psi(\theta_\alpha) \tag{B5}$$

where the density of states $|\nu_\alpha|$ is given in equation (19). A similar expansion holds for ϕ and on applying the operator Ω_+ we get

$$\Omega_+ \phi = \int_{\text{Spec}} d\lambda \sum_{\alpha=1}^{N_\lambda} u_+^{\lambda,\alpha} |\nu_\alpha| \phi(\theta_\alpha). \tag{B6}$$

We now substitute (B5) and (B6) in (B4) and recall that $u_0^{\lambda,\alpha}$ is an eigenfunction of U_0^k corresponding to the eigenvalue $e^{ik\lambda}$. The infinite sum over k in (B4) converges to a δ-function that can be integrated out and we finally get

$$\langle \psi | S\phi \rangle = \langle \psi | \phi \rangle - 2\pi \int_{\text{Spec}} d\lambda \sum_{\alpha,\beta=1}^{N_\lambda} \psi^*(\theta_\alpha) \phi(\theta_\beta) \langle (T-1) u_0^{\lambda,\alpha} | u_+^{\lambda,\beta} \rangle |\nu_\alpha| |\nu_\beta|. \tag{B7}$$

Substituting now expansions (B5) for ψ, ϕ in the left-hand side and in the first term of the right-hand side of (B7) yields equation (24) of the text. Instead, choosing $g = \Omega_- \phi$ in (B2) leads, via quite similar manipulations, to another expression for the S-matrix in which the functions $u_-^{\lambda,\alpha}$ appear

$$S_{\alpha\beta} = \delta_{\alpha\beta} + 2\pi |\nu_\alpha|^{1/2} |\nu_\beta|^{1/2} \langle u_-^{\lambda,\alpha} | (T-1) u_0^{\lambda,\beta} \rangle. \tag{B8}$$

Appendix C: The reciprocity property of the S-matrix

For free waves one has

$$Cu_0^{\lambda,\alpha} = u_0^{\lambda,\alpha^*}$$

where α^* is the reverse channel and C is the complex conjugacy. Because the free dynamics U_0 is time-reversal invariant, the following property holds true for free Green functions:

$$C \lim_{\epsilon \to 0+} (U_0 - e^{i\lambda+\epsilon})^{-1} = \lim_{\epsilon \to 0+} (U_0^{-1} - e^{-i\lambda+\epsilon})^{-1} C.$$

By applying C to both sides of the first Lippmann–Schwinger equation and using this property one gets

$$\left[1 + U_0 \lim_{\epsilon \to 0+} (U_0 - e^{i\lambda-\epsilon})^{-1}(T-1)\right] Cu_+^{\lambda,\beta} = u_0^{\lambda,\beta^*}.$$

Comparing this with (A4) one sees that

$$u_-^{\lambda,\beta^*} = e^{i\lambda} U_0^{-1} C u_+^{\lambda,\beta}. \tag{C1}$$

Substituting (C1) into formula (B8) for the S-matrix leads to the reciprocity property:

$$\begin{aligned} S_{\beta^*\alpha^*} &= \delta_{\alpha\beta} + 2\pi\langle e^{i\lambda} U_0^{-1} C u_+^{\lambda,\beta} | (T-1) u_0^{\lambda,\alpha^*}\rangle \\ &= \delta_{\alpha\beta} + 2\pi\langle C e^{-i\lambda} U_0 u_+^{\lambda,\beta} | C(T^\dagger - 1) u_0^{\lambda,\alpha}\rangle \\ &= \delta_{\alpha\beta} + 2\pi\langle (T^\dagger - 1) u_0^{\lambda,\alpha} | T^\dagger u_+^{\lambda,\beta}\rangle \\ &= \delta_{\alpha\beta} - 2\pi\langle (T-1) u_0^{\lambda,\alpha} | u_+^{\lambda,\beta}\rangle = S_{\alpha\beta} \end{aligned} \tag{C2}$$

where equation (24) has been used in the last line.

Appendix D: Classical transport

The homogeneous boundary-value problem has a complete set of eigenfunctions $u_n(x)$, $(n_0 \leqslant x \leqslant n_0 + L)$. The nth normalized eigenfunction is associated with an eigenvalue λ_n. It has the parity of $(-1)^{n+1}$ under reflections with respect to $\overline{x} = n_0 + L/2$ and it is given by

$$u_n(x) = \begin{cases} \left[\dfrac{L}{2}\left(1 + \dfrac{\sin 2\nu_n}{2\nu_n}\right)\right]^{-1/2} \cos \dfrac{2\nu_n(x-\overline{x})}{L} & (n \text{ odd}) \\ \left[\dfrac{L}{2}\left(1 - \dfrac{\sin 2\nu_n}{2\nu_n}\right)\right]^{-1/2} \sin \dfrac{2\nu_n(x-\overline{x})}{L} & (n \text{ even}). \end{cases} \tag{D1}$$

The eigenvalue equations (9), stem from directly imposing the homogeneous boundary conditions. The solution of the diffusion equation subject to the inhomogeneous boundary conditions is sought in the form:

$$f(x,\tau) = g(x,\tau) + xA(\tau) + B(\tau) \tag{D2}$$

with g satisfying homogeneous conditions and A, B so chosen that (D2) satisfies the complete conditions. Upon expanding the right-hand side of equation (D2) on the basis u_n differential equations for the coefficients of the expansion are obtained that once solved allow to reconstruct $f(x,\tau)$. In the solution thus obtained the coefficients $x_{n,j}$ stem from expanding the functions $F(x) = x$ and $F(x) = 1$ over the basis u_n:

$$x_{n,j} = \begin{cases} \dfrac{a}{\nu_n^2 + a^2 + a} & \text{for odd } n \\ (-1)^j \dfrac{a}{(a^2 + \nu_n^2 + a)(1 + a)} & \text{for even } n. \end{cases}$$

The solution contains a transient part depending on the initial condition. On dropping this part and using equations (5) to calculate the outgoing flux one gets the solution given in the text.

References

Blumel R, Fishman S, Griniasti M and Smilansky U 1986 *Quantum Chaos and Statistical Nuclear Physics (Lecture Notes in Physics vol 263)* (Berlin: Springer) p 212

Blumel R and Smilansky U 1988 *Phys. Rev. Lett.* **60** 477

Bohigas O and Weidenmuller H A 1988 *Ann. Rev. Nucl. Part. Sci.* **38** 421 and references therein

Borgonovi F, Guarneri I and Shepelyansky D L 1991 *Phys. Rev.* A **43** 4517

Brody T A, Flores J, French J B, Mello P A, Pandey A and Wong S S M 1981 *Rev. Mod. Phys.* **53** 385

Buttiker M, Imry Y, Landauer R and Pinhas S 1985 *Phys. Rev.* B **31** 6207

Casati G, Guarneri I and Shepelyansky D L 1990 *Physica* **163A** 205

Eckardt B and Cvitanovic P 1989 *Phys. Rev. Lett.* **63** 823

Fishman S, Grempel D R and Prange R 1982 *Phys. Rev. Lett.* **49** 509

Gaspard P and Rice S A 1989 *J. Chem. Phys.* **90** 2225

Gutzwiller M C 1983 *Physica* **7D** 341

Jalabert R A, Baranger H U and Stone A D 1990 *Phys. Rev. Lett.* **65** 2442

Jung C and Scholz H J 1988 *J. Phys. A: Math. Gen.* **21** 2301

Landauer R 1970 *Phil. Mag.* **21** 863

Lichtenberg A J and Lieberman M A 1983 *Regular and Stochastic Motion (Applied Mathematics Series 38)* (New York: Springer)

Pichard J L 1986 *J. Phys. C: Solid State Phys.* **19** 1519

—— 1990 *Quantum Coherence in Mesoscopic Systems (NATO ASI Series)* ed B Kramer (New York: Plenum)

Prugovechky E 1971 *Quantum Mechanics in Hilbert Space* (New York: Academic)

Rechester A B, Rosenbluth M N and White R B 1981 *Phys. Rev.* A **23** 2264

Shepelyansky D L 1986 *Phys. Rev. Lett.* **56** 677

Smilansky U 1990 *Chaos and Quantum Physics (Lecture Notes for the Les Houches Summer School, Session LII, 1989)* ed M J Giannoni, A Voros and J Zinn-Justin (Amsterdam: North-Holland) and references therein

Vollhardt D 1987 *Festk. Probl.* **27** 63 and references therein